




Cite this: *CrystEngComm*, 2024, 26, 5144

Enhancing the efficiency and stability of electrocatalysts for water splitting: NiCo-LDH nanosheet arrays at high current density

Xiaomei Wang,^a Tiantian Wang,^a Yongren Yu,^a Junhua You,^a Fang Hu ^{*a} and Depeng Zhao^{*b}

The development of low-cost, efficient, and stable bifunctional electrocatalysts is very important for the development of renewable energy. Layered double hydroxides (LDHs) are considered to be promising electrocatalysts due to their flexible ion exchange, abundant structural adjustability, excellent thermal stability, and easy functionalization with other materials. In this work, nickel-cobalt layered double hydroxide (NiCo-LDH) nanosheet arrays are prepared by a simple hydrothermal method. Four samples Ni₁-Co₄-LDH, Ni₂Co₃-LDH, Ni₃Co₂-LDH and Ni₄Co₁-LDH are obtained by adjusting the Ni/Co ratio (5 - x : x). Among them, the Ni₂Co₃-LDH samples show excellent HER and OER properties. At a current density of 50 mA cm⁻² in a 1.0 M KOH electrolyte, the overpotentials of the HER and OER are 227 mV and 303 mV, respectively. In addition, as a bifunctional electrocatalyst for water splitting, the sample provides a voltage of 1.83 V and long-term stability at 50 mA cm⁻².

Received 5th June 2024,
Accepted 6th August 2024

DOI: 10.1039/d4ce00564c

rsc.li/crystengcomm

1. Introduction

With the rapid development of today's social economy, energy consumption is intensifying, and environmental pollution is becoming more and more serious, which makes the development of clean and sustainable energy to replace traditional fossil energy a top priority.¹⁻³ Among the many renewable energy sources, hydrogen energy is considered to be the most promising clean energy due to its high calorific value, pollution-free products, and abundant raw material storage.⁴⁻⁶ In recent years, hydrogen production by water electrolysis has become the focus of researchers, because of its advantages of environmental friendliness, convenient preparation processes, and high product purity.^{7,8} However, its high cost and low energy conversion efficiency have been restricting its commercial development.^{9,10} Water electrolysis for hydrogen production includes the hydrogen evolution reaction (HER) and oxygen evolution reaction (OER).¹¹⁻¹³ In general, proton-coupled electron transfer reactions are slower, and strong O-O double bonds on the anode limit the efficiency of the oxygen evolution reaction (OER).¹⁴⁻¹⁶ In order to improve the conversion efficiency, precious metal catalysts such as Pt-based catalysts, RuO₂ and IrO₂ are widely used. However, due to their scarcity, high cost and weak stability,

they have set up obstacles for their large-scale application.¹⁷ Therefore, the current research hotspot is the development of low-cost, efficient and stable electrocatalysts to accelerate the chemical reaction kinetic process.

According to previous studies, the modification of the catalyst surface, reasonable structural design (such as layered structures and micro-nano arrays) and material composites can achieve the purpose of increasing the number of catalytic activity reaction sites, enhancing the reaction activity and improving the catalytic performance.¹⁸⁻²⁰ Nickel foam (NF) is often used as a substrate due to its high porosity and good electrical conductivity, and combined with the controlled growth technology of two-dimensional layered double hydroxide (LDH), it is possible to prepare high-efficiency and high-stability non-precious metal catalysts.^{21,22} Non-noble metal electrocatalysts, represented by transition metal LDH, have been widely studied because of their unique layered structure and relatively open ion diffusion rates.^{23,24} Compared with a single transition metal, bimetallic hydroxides can expose more reactive sites to promote the occurrence of reactions and accelerate the diffusion of ions.^{25,26} Therefore, bimetallic hydroxides have better catalytic properties. Among many metallic elements, nickel and cobalt are transition metal elements, and Ni-Co-based catalysts have become the focus of research due to their low price, abundant reserves, and excellent hydrogen and oxygen evolution performance in alkaline environments. In recent years, Bao *et al.* had prepared CoMo-LDH ultra-thin nanosheets by the co-precipitation method, and the

^a School of Materials Science and Engineering, Shenyang University of Technology, Shenyang 110870, P. R. China. E-mail: hufang25@126.com, youjunhua168@163.com

^b School of Renewable Energy, Shenyang Institute of Engineering, Shenyang, 110136, P. R. China. E-mail: Hellodepeng@163.com

electronic structure of LDH had been changed due to the doping of Mo⁶⁺, which had promoted the occurrence of catalytic reactions.²⁷ At a current density of 10 mA cm⁻², the OER and HER overpotentials were 290 mV and 115 mV, respectively. Song *et al.* prepared CoMn-LDH ultrathin nanoplates, and the reaction rate was more than 20 times that of Co(OH)₂.²⁸ All of them exhibited better catalytic activity than monometallic hydroxide Co(OH)₂. Ye *et al.* used a simple one-step hydrothermal method to prepare a novel two-dimensional NiCr-LDH nanosheet array with a three-dimensional porous structure, which has excellent durability and exhibits efficient and stable electrocatalytic activity in alkaline media.²⁹ To date, many studies have promoted the understanding and progress of TM LDH nanosheets as electrocatalysts. However, there are still many challenges in optimizing the electrocatalytic performance of TM LDHs, which limits their further commercial electrocatalytic applications.^{30,31}

Herein, we grow NiCo-LDH nanosheet arrays *in situ* on nickel foam (NF) by a simple hydrothermal method, and the samples prepared by adjusting the ratio of Ni to Co (Ni:Co = 5 - x:x) are denoted as Ni₁Co₄-LDH, Ni₂Co₃-LDH, Ni₃Co₂-LDH and Ni₄Co₁-LDH, respectively. Through structural characterization and electrochemical performance testing, it can be found that Ni₂Co₃-LDH/NF exhibits excellent electrocatalytic performance. The HER overpotentials at 50 mA cm⁻² are 227 mV and 303 mV in a 1.0 M KOH electrolyte and excellent stability after 12 h of cycling is maintained.

2. Experiment

Before the experiment, a piece of nickel foam was washed with absolute ethanol and deionized water. NiCo-LDH was synthesized on nickel foam (NF) by a simple hydrothermal method. Firstly, NiCl₂·6H₂O and Co(NO₃)₂·6H₂O were dissolved in a mixture of 60 mL of methanol and deionized water (1:1) according to the molar ratio (5 - x:x) and stirred for 30 min. Then, 3 mM urea was added to the above solution during constant stirring. Finally, the above mixture and pretreated nickel foam (4 × 4 cm) were transferred to a 100 mL reactor and kept at 140 °C for 6 hours. After natural cooling to room temperature, the prepared samples were washed with absolute ethanol and deionized water and dried overnight at 60 °C to prepare NiCo-LDH samples with different Ni/Co ratios. All reagents are of analytical-grade and require no further purification.

Structure characterization

X-ray diffraction (XRD, Shimadzu-7000, Cu Kα), X-ray photoelectron spectroscopy (XPS ESCALAB 250 with Al Kα radiation), scanning electron microscopy (SEM, Gemini 300-71-31), and transmission electron microscopy (TEM, JEM-2100 PLUS) were used to characterize the morphology and crystal structure of the samples in detail.

Electrochemical performance testing

An electrochemical workstation was used to measure the electrochemical performance of a sample. The electrolyte was 1.0 M KOH in aqueous solution, using a standard three-electrode system, the counter electrode was 1 cm² platinum sheet, the reference electrode was Ag/AgCl, and the working electrode was NiCo-LDH/NF; linear scanning voltammetry (LSV), electrochemical impedance (EIS), cyclic voltammetry (CV), and chronopotentiometry (CP) were performed. According to the Nernst equation $E_{\text{RHE}} = E_{\text{Ag/AgCl}} + 0.197 \text{ V} + 0.059 \text{ V} \times \text{pH}$, all potentials can be converted into reversible hydrogen electrodes (RHEs). The overpotential is $\eta = E_{\text{RHE}} - 1.23 \text{ V}$.

3. Results and discussion

First, the prepared samples are characterized by XRD. As shown in Fig. 1a, the angles of the strong diffraction peaks at 2θ are 11.718, 23.242, 34.108, and 38.309 degrees, which belong to the (003), (006), (012), and (015) crystal planes of the NiCo-LDH phase (JCPDS number: 40-0216). The remaining peaks are 44.622 and 60.054 degrees, belonging to the (260) and (444) planes (JCPDS number: 47-0938). This result strongly proves that NiCo-LDH can be successfully prepared on NF. Fourier transform infrared spectroscopy (FTIR) was conducted to further investigate the structural characteristics of the samples (Fig. 1b); 3518 cm⁻² and 1600 cm⁻² correspond to O–H bonds, 1000–800 cm⁻² correspond to M (metal)–O bonds,³² and 2912 cm⁻² and 2198 cm⁻² correspond to C–H bonds. In addition to this, 1367 cm⁻² and 1605 cm⁻² correspond to the C=C bond.³³ This further indicates the successful preparation of Ni_xCo_y-LDH.

Next, the elemental composition and chemical state of the Ni₂Co₃-LDH product are investigated by XPS. The full XPS spectrum of Ni_xCo_y-LDH/NF is shown in Fig. 1c, indicating the presence of elements such as Ni, Co, C, and O in the prepared sample. As shown in Fig. 1d, the binding energies of Ni 2p_{3/2} and Ni 2p_{1/2} for Ni²⁺ correspond to the peaks at 854.00 eV and 871.31 eV, and those of Ni 2p_{3/2} and Ni 2p_{1/2} for Ni³⁺ correspond to the peaks at 856.09 eV and 873.78 eV, indicating the coexistence of Ni²⁺ and Ni³⁺ ions in the prepared product.³⁴ In addition, the binding energies at the satellite peaks are 860.71 eV and 878.26 eV. In the Ni 2p spectrum, the binding energy of Ni³⁺ is higher than that of Ni²⁺, indicating that Ni³⁺ is the dominant valence state. The Co 2p spectrum (Fig. 1e) can be fitted to Co³⁺ and Co²⁺; the binding energies of 780.00 eV and 796.49 eV belong to Co³⁺, and the binding energies of 782.66 eV and 800.34 eV belong to Co²⁺, and the two satellite peaks of Co are located at 786.54 eV and 803.05 eV. These results confirm the coexistence of Co³⁺ and Co²⁺ and the high atomic ratio of Co³⁺.³⁵ The O 1s spectrum consists of two characteristic peaks, 529.7 eV and 531.09 eV, which are attributed to metal–oxygen bonds (M–O) and oxygen vacancies (V_O), respectively, as shown in Fig. 1f.³⁶

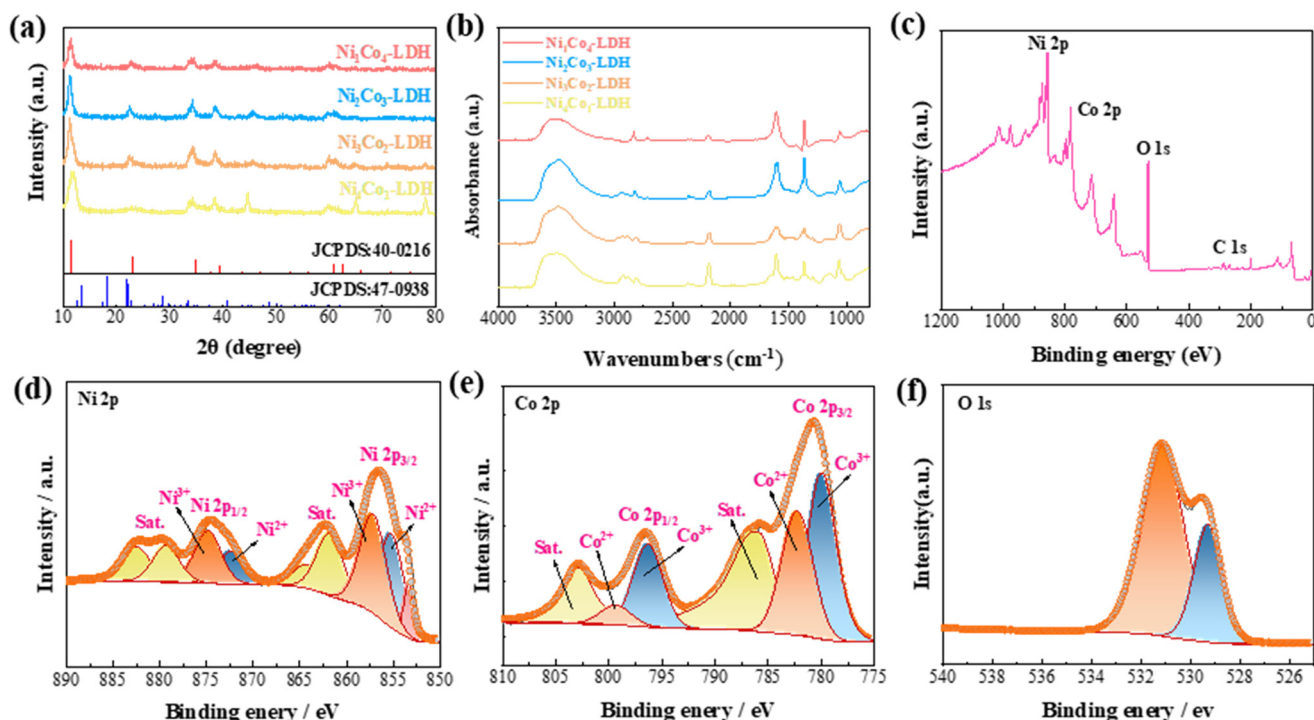


Fig. 1 (a) XRD spectra of $\text{Ni}_x\text{Co}_y\text{-LDH}$; (b) FTIR spectra of $\text{Ni}_x\text{Co}_y\text{-LDH}$; (c) XPS spectra of $\text{Ni}_x\text{Co}_y\text{-LDH}$ and (d) Ni 2p; (e) Co 2p; (f) O 1s.

Scanning electron microscopy (SEM) is used to characterize the topography of the sample, as shown in Fig. 2(a) and (b). As you can see, the nanosheets are evenly staggered on the surface of the NF, with an average thickness of 90 nm. This array and the resulting porous nanostructures facilitate the diffusion of ions and the transport of charges. The elemental energy spectrum (EDS) of the sample (Fig. 2c) shows a uniform distribution of the Ni, Co, O, and C elements. Fig. 2(d) and (e) show local TEM images of the

nanoflower $\text{Ni}_x\text{Co}_y\text{-LDH}$ formed by the combination of many ultrathin nanosheet arrays, further demonstrating the lamellar formation of the nanosheet array. Fig. 2f shows the corresponding HRTEM image with a plane spacing of 0.256 nm that matches well with the (012) plane.

The OER performance of the samples is investigated in a 1.0 M KOH electrolyte.

Fig. 3a shows the LSV curves for all catalysts at 2 mV s^{-1} . At 50 mA cm^{-2} , the overpotential of the $\text{Ni}_2\text{Co}_3\text{-LDH}$

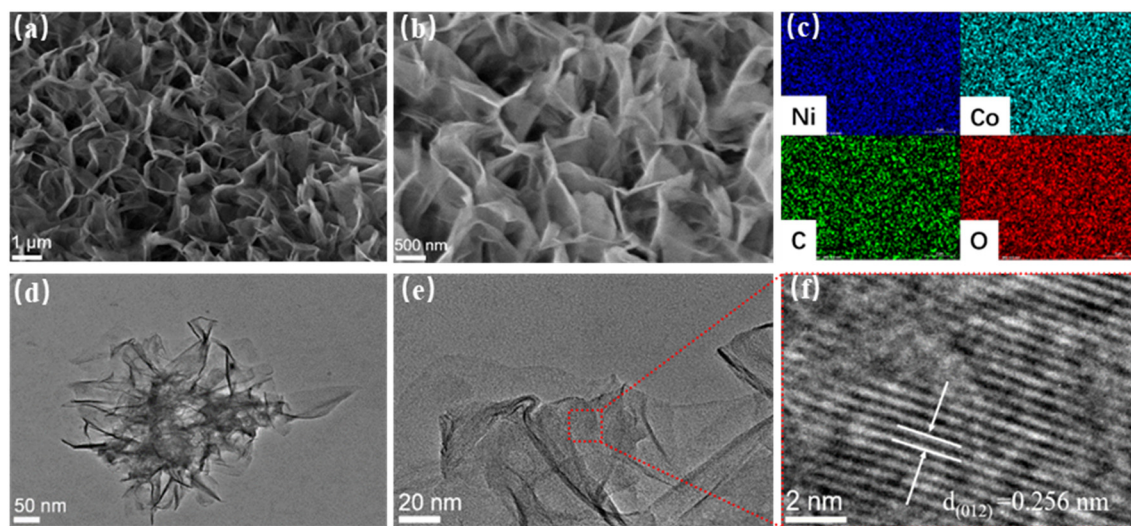


Fig. 2 Morphology and structure characterization of $\text{Ni}_2\text{Co}_3\text{-LDH}$ samples. (a) Low-magnification SEM images; (b) high-magnification SEM images; (c) EDS element mapping; (d) and (e) TEM images; (f) HRTEM image.

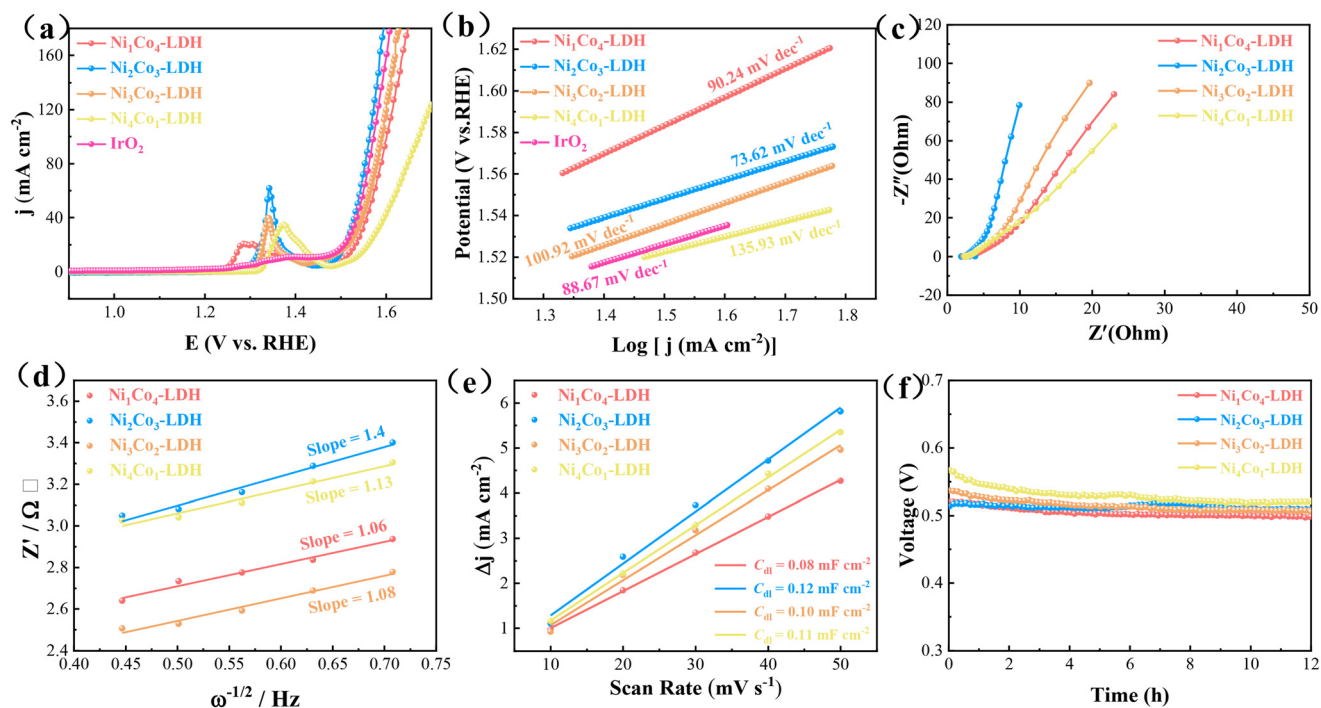


Fig. 3 OER performance. (a) Polarization curve at a scan rate of 2 mV s^{-1} ; (b) Tafel diagram; (c) Nyquist plots; (d) impedance fitting of four samples; (e) linear fit of electric double-layer capacitance (C_{dl}) measurements; (f) constant voltage cycle diagram.

sample is 303 mV, less than that of $\text{Ni}_1\text{Co}_4\text{-LDH}$ (339 mV), $\text{Ni}_3\text{Co}_2\text{-LDH}$ (335 mV), $\text{Ni}_4\text{Co}_1\text{-LDH}$ (381 mV) and IrO_2 (313 mV). The results show that the activation energy required for the $\text{Ni}_2\text{Co}_3\text{-LDH}$ reaction is lower and the kinetic rate of the reaction is faster. The Tafel plot (Fig. 3b) is used to reflect the OER kinetics of the prepared samples, and the Tafel slope of $\text{Ni}_2\text{Co}_3\text{-LDH}$ is $73.62 \text{ mV dec}^{-1}$, which is significantly lower than those of $\text{Ni}_1\text{Co}_4\text{-LDH}$ ($90.24 \text{ mV dec}^{-1}$), $\text{Ni}_3\text{Co}_2\text{-LDH}$ ($100.92 \text{ mV dec}^{-1}$), $\text{Ni}_4\text{Co}_1\text{-LDH}$ ($135.93 \text{ mV dec}^{-1}$) and IrO_2 ($88.67 \text{ mV dec}^{-1}$). The results show that the sample $\text{Ni}_2\text{Co}_3\text{-LDH}$ has a higher electron and ion transfer velocity. Electrochemical impedance spectroscopy (EIS) is performed in the frequency range of 100 kHz to 0.1 Hz to further investigate the $\text{Ni}_x\text{Co}_y\text{-LDH}$ electrode reaction kinetics (Fig. 3c). In Fig. 3d, the slope value of the $\text{Ni}_2\text{Co}_3\text{-LDH}$ electrode is 1.4, which is higher than those of $\text{Ni}_1\text{Co}_4\text{-LDH}$ (1.06), $\text{Ni}_3\text{Co}_2\text{-LDH}$ (1.08), and $\text{Ni}_4\text{Co}_1\text{-LDH}$ (1.13), indicating that the $\text{Ni}_2\text{Co}_3\text{-LDH}$ sample can provide a faster channel for ions than the other three samples. $\text{Ni}_2\text{Co}_3\text{-LDH}$ exhibits smaller equivalent resistance than $\text{Ni}_1\text{Co}_4\text{-LDH}$, $\text{Ni}_3\text{Co}_2\text{-LDH}$ and $\text{Ni}_4\text{Co}_1\text{-LDH}$, indicating that the $\text{Ni}_2\text{Co}_3\text{-LDH}$ electrode has excellent conductivity. The electrochemically active surface area (ECSA) is an effective parameter for further investigating catalyst catalytic activity, which is calculated in terms of double-layer capacitance (C_{dl}), as shown in Fig. 3e. The C_{dl} value of $\text{Ni}_2\text{Co}_3\text{-LDH}$ is 0.12 mF cm^{-2} , higher than those of $\text{Ni}_1\text{Co}_4\text{-LDH}$ (0.08 mF cm^{-2}), $\text{Ni}_3\text{Co}_2\text{-LDH}$ (0.10 mF cm^{-2}) and $\text{Ni}_4\text{Co}_1\text{-LDH}$ (0.11 mF cm^{-2}). A higher C_{dl} value represents a larger electrochemically active surface area. Stability is

another important criterion that affects the performance of catalysts. Therefore, Fig. 3f shows the long-term OER cycling stability of the four samples prepared. Among them, the $\text{Ni}_2\text{Co}_3\text{-LDH}$ catalyst can maintain good stability for up to 12 hours.

The HER performance of the samples is investigated using LSV curves, as shown in Fig. 4a. At -50 mA cm^{-2} , the overpotential (227.00 mV) of the $\text{Ni}_2\text{Co}_3\text{-LDH}$ sample is lower than those of the $\text{Ni}_1\text{Co}_4\text{-LDH}$ sample (278.7 mV), the $\text{Ni}_3\text{Co}_2\text{-LDH}$ sample (251.59 mV), and the $\text{Ni}_4\text{Co}_1\text{-LDH}$ sample (265.7 mV), respectively. The overpotential of commercial Pt/C is 85.7 mV. The corresponding Tafel curves (Fig. 4b) show that the Tafel slope of $\text{Ni}_2\text{Co}_3\text{-LDH}$ is $99.46 \text{ mV dec}^{-1}$, lower than those of $\text{Ni}_1\text{Co}_4\text{-LDH}$ ($207.56 \text{ mV dec}^{-1}$), $\text{Ni}_3\text{Co}_2\text{-LDH}$ ($126.36 \text{ mV dec}^{-1}$), and $\text{Ni}_4\text{Co}_1\text{-LDH}$ ($205.59 \text{ mV dec}^{-1}$). Commercial Pt/C exhibits the smallest Tafel slope ($63.44 \text{ mV dec}^{-1}$). The results show that the sample $\text{Ni}_2\text{Co}_3\text{-LDH}$ has a rapid HER reaction kinetics.

The charge transfer kinetics is then investigated by electron diffraction spectroscopy (Fig. 4c), and it can be seen that the semicircular diameter of the $\text{Ni}_2\text{Co}_3\text{-LDH}$ sample is smaller than those of the other three samples, indicating that the $\text{Ni}_2\text{Co}_3\text{-LDH}$ catalyst has excellent conductivity. The slope value of the $\text{Ni}_2\text{Co}_3\text{-LDH}$ electrode is 94.49, which is higher than those of $\text{Ni}_1\text{Co}_4\text{-LDH}$ (49.73), $\text{Ni}_3\text{Co}_2\text{-LDH}$ (53.18) and $\text{Ni}_4\text{Co}_1\text{-LDH}$ (10.02), showing its high ion diffusion ability (Fig. 4d). Fig. 4e shows the electrochemically active surface area (ECSA) of the sample. The C_{dl} value of $\text{Ni}_2\text{Co}_3\text{-LDH}$ is 0.012 mF cm^{-2} , which is higher than those of $\text{Ni}_1\text{Co}_4\text{-LDH}$ (0.007 mF cm^{-2}), $\text{Ni}_3\text{Co}_2\text{-LDH}$ (0.008 mF cm^{-2}) and $\text{Ni}_4\text{Co}_1\text{-LDH}$

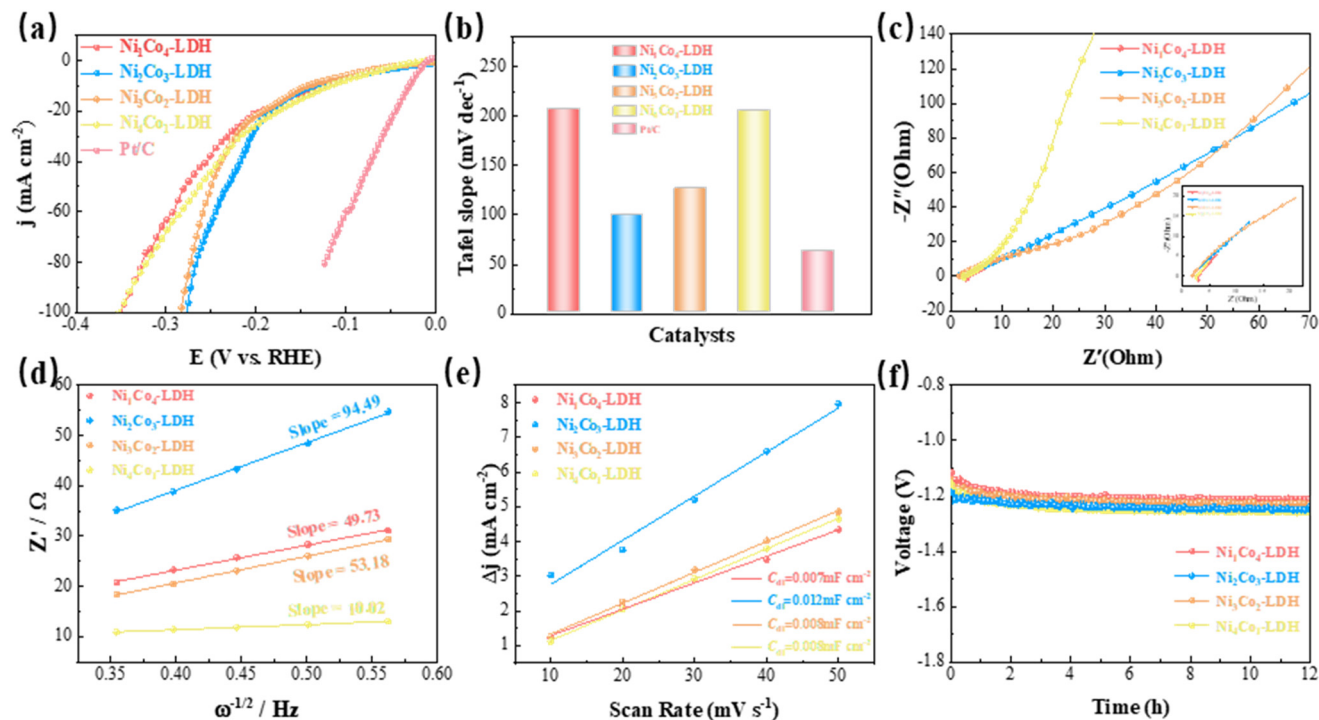


Fig. 4 HER performance. (a) LSV curve at 5 mV s^{-1} ; (b) Tafel diagram; (c) Nyquist diagram; (d) impedance fitting curve; (e) electric double-layer capacitance (C_{dl}); (f) 12 hour constant voltage stability.

LDH (0.008 mF cm^{-2}). Fig. 4f shows the cycling stability of the prepared sample catalyst. Among them, the Ni_2Co_3 -LDH catalyst has better durability.

We then perform a structural analysis on the Ni_2Co_3 -LDH samples that have undergone cyclic testing. First, XPS is used to analyze the surface valence state of the sample. As shown

in Fig. 5a, the peaks at 855.68 eV and 874.68 eV in the Ni 2p spectrum are attributed to Ni^{3+} , with Ni^{2+} corresponding to the peaks at 855.65 eV and 871.98 eV binding energies.³⁷ The binding energies of the corresponding peaks of Co^{3+} in the Co 2p spectrum (Fig. 5b) are 779.58 eV and 794.8 eV , and the corresponding peaks of Co^{2+} are 782.9 eV and 796.8 eV .³⁸ The

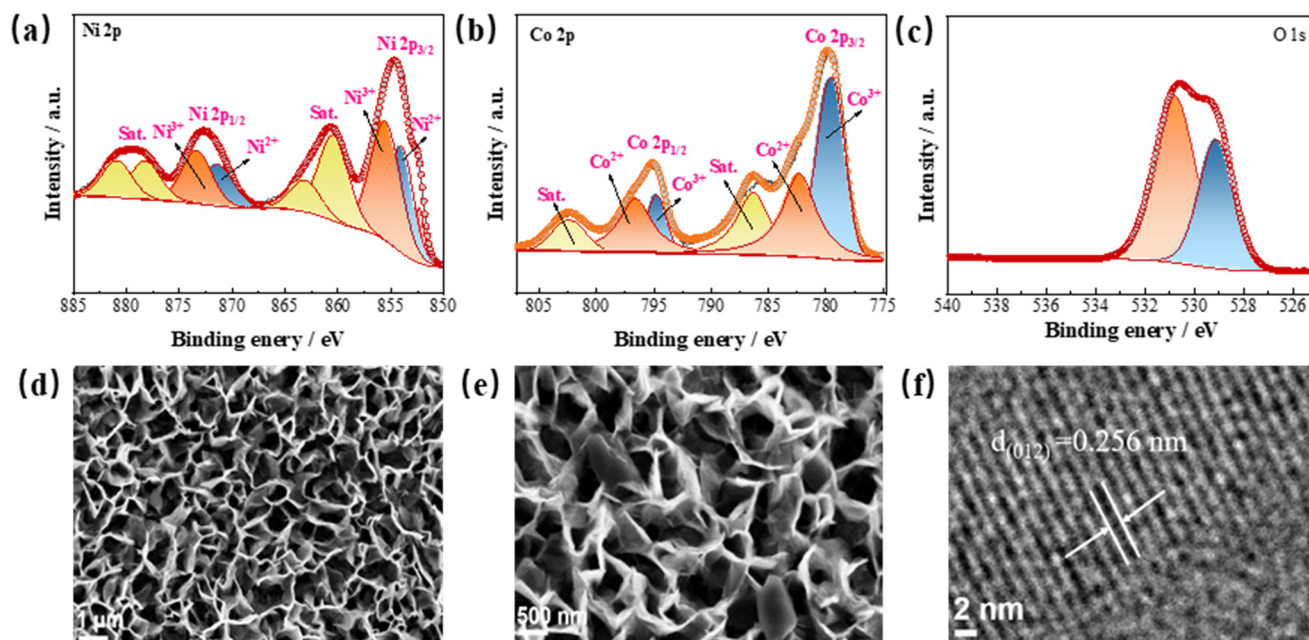


Fig. 5 Morphology and structure characterization of the Ni_2Co_3 -LDH catalyst after OER cycling. (a) Ni 2p XPS; (b) Co 2p XPS; (c) O 1s XPS; (d) low-magnification SEM image; (e) high-magnification SEM image; (f) HRTEM image.

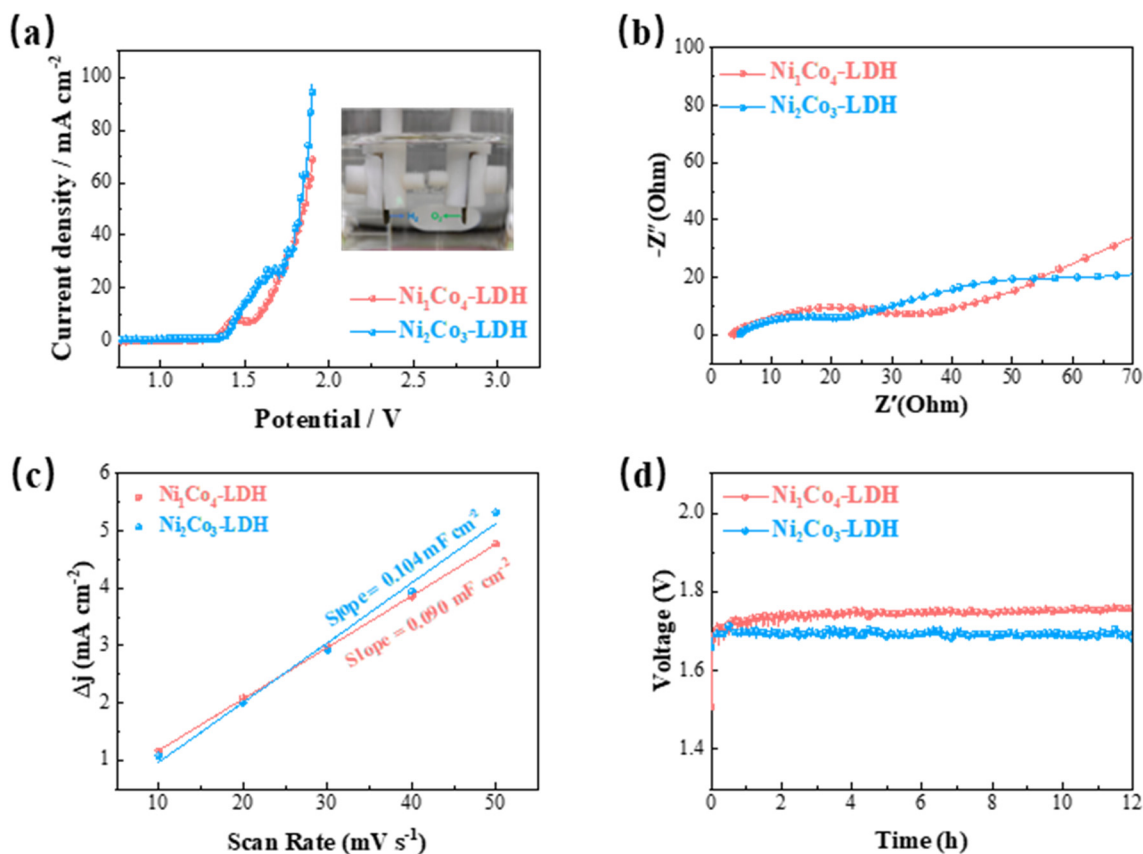


Fig. 6 (a) Polarization curve of the catalyst with a scan rate of 5 mV s^{-1} ; (b) Nyquist curve of overall hydrolysis; (c) double layer capacitance for fully soluble water; (d) cycling data for overall water splitting.

O 1s spectrum (Fig. 5c) contains two peaks, a metal–oxygen bond (529.09 eV) and an oxygen ion (530.8 eV).³⁹ The above results show that the position and relative intensity of the XPS peak remain basically unchanged, indicating the chemical stability of the Ni, Co and O components. The XPS data confirms that the three metal elements are still in the trimetal LDH system after cyclic testing, and the composition of $\text{Ni}_2\text{Co}_3\text{-LDH}$ is stable. The morphology and structure of the cycled $\text{Ni}_2\text{Co}_3\text{-LDH}$ samples are studied. From the SEM images (Fig. 5d and e), the layered morphology of the nanosheet array can still be maintained in the samples after cycling, indicating that the above catalysts have excellent structural stability. As can be seen in Fig. 5f, the lattice spacing of the HRTEM image is 0.256 nm, which is well matched to the (012) plane. It shows that the structure of the sample does not change significantly after cycling.

Finally, the overall hydrolysis performance of NiCo-LDH is studied. Fig. 6a shows the LSV curve of $\text{Ni}_x\text{Co}_y\text{-LDH}$ at a scan rate of 5 mV s^{-1} . Compared to $\text{Ni}_1\text{Co}_4\text{-LDH}$ (1.85 V), the application voltage of the $\text{Ni}_2\text{Co}_3\text{-LDH}$ sample (1.83 V) is lower at 50 mA cm^{-2} . As the electrolytic reaction progresses, the cathode (H_2) and anode (O_2) produce many bubbles. The EIS plot (Fig. 6b) shows that the $\text{Ni}_2\text{Co}_3\text{-LDH}$ sample exhibits a smaller semicircular diameter in the high-frequency region

and a larger slope in the low-frequency region compared to the $\text{Ni}_1\text{Co}_4\text{-LDH}$ sample. This phenomenon indicates that the $\text{Ni}_2\text{Co}_3\text{-LDH}$ sample has high electrical conductivity. In the total solution water system, the C_{dl} value of $\text{Ni}_2\text{Co}_3\text{-LDH}$ (0.104 mF cm^{-2}) is higher than that of $\text{Ni}_1\text{Co}_4\text{-LDH}$ (0.090 mF cm^{-2}), suggesting that more exposed active sites existed in the sample $\text{Ni}_2\text{Co}_3\text{-LDH}$ and it exhibited superior catalytic activity as shown in Fig. 6c. To test the cycling stability of the samples, a chronopotentiometric method (CP) is employed, as shown in Fig. 6d. The results show that the current density of the $\text{Ni}_2\text{Co}_3\text{-LDH}$ catalyst is more stable than that of the $\text{Ni}_1\text{Co}_4\text{-LDH}$ catalyst after cycling up to 12 h, indicating that the $\text{Ni}_2\text{Co}_3\text{-LDH}$ catalyst has excellent water splitting performance.

4. Conclusion

In summary, we synthesize a novel two-dimensional $\text{Ni}_x\text{Co}_y\text{-LDH}$ nanosheet array with a three-dimensional porous structure on nickel foam (NF) by a simple hydrothermal method. The $\text{Ni}_2\text{Co}_3\text{-LDH}$ electrocatalyst exhibits excellent HER and OER properties, and is a highly efficient and stable bifunctional catalyst. At a current density of 50 mA cm^{-2} , $\text{Ni}_2\text{-Co}_3\text{-LDH}$ has an overpotential of 227 mV in the HER and 303 mV in the OER, and has excellent cycling stability in alkaline

electrolytes. In addition, Ni₂Co₃-LDH exhibits excellent electrocatalytic performance. It can be efficiently hydrolyzed at a current density of 50 mA cm⁻² at 1.83 V and has long-term durability. Its excellent performance may be related to the special spatial structure, sufficient interfacial reactions, and the synergy between the components. This further expands the scope of non-precious metal electrocatalysts for efficient water splitting.

Data availability

Data are available on request from the authors.

Conflicts of interest

The authors declare no conflict of interest.

Acknowledgements

This work was financially supported by the Liaoning Applied Basic Research Program (No. 2023JH2/101300011, No. 2023JH2/101300018), the Basic Scientific Research Project of Liaoning Province Department of Education (No. LJKZZ20220024), and the Shenyang Science and Technology Project (No. 23-407-3-13).

References

- 1 Y. Gong, J. Yao and P. Wang, et al., Perspective of hydrogen energy and recent progress in electrocatalytic water splitting[J], *Chin. J. Chem. Eng.*, 2022, **43**, 282–296.
- 2 J. Wang, P. Chen and S. Ruan, et al., Construction and optimization of multi-interface nanotube structured phosphorus-doped bimetallic oxide arrays as efficient electrocatalysts for water splitting[J], *CrystEngComm*, 2024, **26**(20), 2692–2703.
- 3 L. Tian, Y. Liu and C. He, et al., Hollow heterostructured nanocatalysts for boosting electrocatalytic water splitting[J], *Chem. Rec.*, 2023, **23**(2), e202200213.
- 4 J. Gu, Y. Peng and T. Zhou, et al., Porphyrin-based framework materials for energy conversion[J], *Nano Res. Energy*, 2022, **1**, e9120009.
- 5 W. R. Yan, Y. Xue and M. C. Liu, et al., Room temperature and rapid synthesis of two-dimensional bimetallic NiCo-CAT MOFs by an electrochemical strategy for enhancing electrocatalytic oxygen evolution reaction[J], *CrystEngComm*, 2024, **26**, 3185.
- 6 J. Gu, Y. Peng and T. Zhou, et al., Porphyrin-based framework materials for energy conversion[J], *Nano Res. Energy*, 2022, **1**, e9120009.
- 7 M. Chatenet, B. G. Pollet and D. R. Dekel, et al., Water electrolysis: from textbook knowledge to the latest scientific strategies and industrial developments[J], *Chem. Soc. Rev.*, 2022, **51**(11), 4583–4762.
- 8 J. Xie, X. Zhang and H. Zhang, et al., Intralayered Ostwald Ripening to Ultrathin Nanomesh Catalyst with Robust Oxygen-Evolving Performance[J], *Adv. Mater.*, 2017, **29**(10), 1604765.
- 9 B. Feng, S. Jin and J. Lang, et al., FeS nanosheets assembled with 1T-MoS₂ nanoflowers on iron foam for efficient overall water splitting[J], *CrystEngComm*, 2024, **26**(17), 2269–2276.
- 10 C. Ye, L. Zhang and L. Yue, et al., A NiCo LDH nanosheet array on graphite felt: an efficient 3D electrocatalyst for the oxygen evolution reaction in alkaline media[J], *Inorg. Chem. Front.*, 2021, **8**(12), 3162–3166.
- 11 G. Givirovskiy, V. Ruuskanen and T. Väkiparta, et al., Electrocatalytic performance and cell voltage characteristics of 1st-row transition metal phosphate (TM-Pi) catalysts at neutral pH[J], *Mater. Today Energy*, 2020, **17**, 100426.
- 12 H. Bai, D. Chen and Q. Ma, et al., Atom doping engineering of transition metal phosphides for hydrogen evolution reactions[J], *Electrochem. Energy Rev.*, 2022, **5**(2), 24.
- 13 J. Yuan, J. Zhou and Z. Peng, et al., Enhanced electrocatalytic hydrogen evolution in alkaline saline electrolyte by NiCo foam supported iridium nanoclusters[J], *J. Mater. Chem. A*, 2024, **12**(4), 2383–2390.
- 14 D. Zhao, M. Dai and H. Liu, et al., PPy film anchored on ZnCo₂O₄ nanowires facilitating efficient bifunctional electrocatalysis[J], *Mater. Today Energy*, 2021, **20**, 100637.
- 15 Y. Guo, T. Park and J. W. Yi, et al., Nanoarchitectonics for transition-metal-sulfide-based electrocatalysts for water splitting[J], *Adv. Mater.*, 2019, **31**(17), 1807134.
- 16 Y. Sun, R. Li and X. Chen, et al., A-site management prompts the dynamic reconstructed active phase of perovskite oxide OER catalysts[J], *Adv. Energy Mater.*, 2021, **11**(12), 2003755.
- 17 Q. Wang, X. Huang and Z. L. Zhao, et al., Ultrahigh-loading of Ir single atoms on NiO matrix to dramatically enhance oxygen evolution reaction[J], *J. Am. Chem. Soc.*, 2020, **142**(16), 7425–7433.
- 18 M. Wang, X. Liu and Y. Sun, et al., High-efficiency NiCo layered double hydroxide electrocatalyst[J], *New J. Chem.*, 2022, **46**(38), 18535–18542.
- 19 P. Wang, Y. Luo and G. Zhang, et al., Interface engineering of Ni_xS_y@MnO_xH_y nanorods to efficiently enhance overall-water-splitting activity and stability[J], *Nano-Micro Lett.*, 2022, **14**(1), 120.
- 20 X. W. Lv, W. W. Tian and Z. Y. Yuan, Recent advances in high-efficiency electrocatalytic water splitting systems[J], *Electrochem. Energy Rev.*, 2023, **6**(1), 23.
- 21 J. Yan, L. Chen and X. Liang, Co₉S₈ nanowires@NiCo-LDH nanosheets arrays on nickel foams towards efficient overall water splitting[J], *Sci. Bull.*, 2019, **64**(3), 158–165.
- 22 J. Hou, Y. Wu and S. Cao, et al., Active sites intercalated ultrathin carbon sheath on nanowire arrays as integrated core-shell architecture: highly efficient and durable electrocatalysts for overall water splitting[J], *Small*, 2017, 1702018.
- 23 Z. Wu, Q. Li and G. Xu, et al., Microwave Phosphine-Plasma-Assisted Ultrafast Synthesis of Halogen-Doped Ru/RuP₂ with Surface Intermediate Adsorption Modulation for Efficient Alkaline Hydrogen Evolution Reaction[J], *Adv. Mater.*, 2024, **36**(13), 2311018.
- 24 H. Yu, W. Wang and Q. Mao, et al., Pt single atom captured by oxygen vacancy-rich NiCo layered double

- hydroxides for coupling hydrogen evolution with selective oxidation of glycerol to formate[J], *Appl. Catal., B*, 2023, **330**, 122617.
- 25 B. Wang, J. Li and D. Li, *et al.*, Single atom iridium decorated nickel alloys supported on segregated MoO₂ for alkaline water electrolysis[J], *Adv. Mater.*, 2024, **36**(11), 2305437.
- 26 X. Tan, Z. Duan and H. Liu, *et al.*, Core-shell structured MoS₂/Ni₉S₈ electrocatalysts for high performance hydrogen and oxygen evolution reactions[J], *Mater. Res. Bull.*, 2022, **146**, 111626.
- 27 J. Bao, Z. Wang and J. Xie, *et al.*, The CoMo-LDH ultrathin nanosheet as a highly active and bifunctional electrocatalyst for overall water splitting[J], *Inorg. Chem. Front.*, 2018, **5**(11), 2964–2970.
- 28 F. Song and X. Hu, Ultrathin cobalt–manganese layered double hydroxide is an efficient oxygen evolution catalyst[J], *J. Am. Chem. Soc.*, 2014, **136**(47), 16481–16484.
- 29 W. Ye, X. Fang and X. Chen, *et al.*, A three-dimensional nickel–chromium layered double hydroxide micro/nanosheet array as an efficient and stable bifunctional electrocatalyst for overall water splitting[J], *Nanoscale*, 2018, **10**(41), 19484–19491.
- 30 J. Cai, Y. Song and Y. Zang, *et al.*, N-induced lattice contraction generally boosts the hydrogen evolution catalysis of P-rich metal phosphides[J], *Sci. Adv.*, 2020, **6**(1), eaaw8113.
- 31 Y. Zhao, Z. Niu and J. Zhao, *et al.*, Recent advancements in photoelectrochemical water splitting for hydrogen production[J], *Electrochem. Energy Rev.*, 2023, **6**(1), 14.
- 32 H. W. Chen and C. Li, PEDOT: fundamentals and its nanocomposites for energy storage[J], *Chin. J. Polym. Sci.*, 2020, **38**(5), 435–448.
- 33 H. Liu, D. Zhao and M. Dai, *et al.*, PEDOT decorated CoNi₂S₄ nanosheets electrode as bifunctional electrocatalyst for enhanced electrocatalysis[J], *Chem. Eng. J.*, 2022, **428**, 131183.
- 34 X. Wang, H. Song and S. Ma, *et al.*, Template ion-exchange synthesis of Co-Ni composite hydroxides nanosheets for supercapacitor with unprecedented rate capability[J], *Chem. Eng. J.*, 2022, **432**, 134319.
- 35 H. Jia, Z. Wang and X. Zheng, *et al.*, Interlaced Ni-Co LDH nanosheets wrapped Co₉S₈ nanotube with hierarchical structure toward high performance supercapacitors[J], *Chem. Eng. J.*, 2018, **351**, 348–355.
- 36 W. Liang, M. Wang and C. Ma, *et al.*, NiCo-LDH Hollow Nanocage Oxygen Evolution Reaction Promotes Luminol Electrochemiluminescence[J], *Small*, 2023, 2306473.
- 37 Y. Yang, L. Dang and M. J. Shearer, *et al.*, Highly active trimetallic NiFeCr layered double hydroxide electrocatalysts for oxygen evolution reaction[J], *Adv. Energy Mater.*, 2018, **8**(15), 1703189.
- 38 S. Yao, Y. Jiao and C. Lv, *et al.*, Lattice-strain engineering of CoOOH induced by NiMn-MOF for high-efficiency supercapacitor and water oxidation electrocatalysis[J], *J. Colloid Interface Sci.*, 2022, **623**, 1111–1121.
- 39 W. Guo, C. Dun and C. Yu, *et al.*, Mismatching integration-enabled strains and defects engineering in LDH microstructure for high-rate and long-life charge storage[J], *Nat. Commun.*, 2022, **13**(1), 140.